The effects of size and synthesis methods of gold nanoparticle-conjugated MαHIgG$_4$ for use in an immunochromatographic strip test to detect brugian filariasis

2012 Nanotechnology 23 495719

(http://iopscience.iop.org/0957-4484/23/49/495719)

Nanotechnology **23** (2012) 495719 (13pp) doi:10.1088/0957-4484/23/49/495719

The effects of size and synthesis methods of gold nanoparticle-conjugated MαHIgG$_4$ for use in an immunochromatographic strip test to detect brugian filariasis

Siti Rabizah Makhsin[1], Khairunisak Abdul Razak[1,2], Rahmah Noordin[2], Nor Dyana Zakaria[2] and Tan Soo Chun[2]

[1] School of Materials and Mineral Resources Engineering, Universiti Sains Malaysia, 14300 Nibong Tebal, Penang, Malaysia
[2] Nanobiotechnology Research and Innovation (NanoBRI), Institute for Research in Molecular Medicine, Universiti Sains Malaysia, 11800 Penang, Malaysia

E-mail: khairunisak@eng.usm.my

Received 30 July 2012, in final form 1 October 2012
Published 19 November 2012
Online at stacks.iop.org/Nano/23/495719

Abstract
This study describes the properties of colloidal gold nanoparticles (AuNPs) with sizes of 20, 30 and 40 nm, which were synthesized using citrate reduction or seeding-growth methods. Likewise, the conjugation of these AuNPs to mouse anti-human IgG$_4$ (MαHIgG$_4$) was evaluated for an immunochromatographic (ICG) strip test to detect brugian filariasis. The morphology of the AuNPs was studied based on the degree of ellipticity (G) of the transmission electron microscopy images. The AuNPs produced using the seeding-growth method showed lower ellipticity ($G \leq 1.11$) as compared with the AuNPs synthesized using the citrate reduction method ($G \leq 1.18$). Zetasizer analysis showed that the AuNPs that were synthesized using the seeding-growth method were almost monodispersed with a lower polydispersity index (PDI; PDI ≤ 0.079), as compared with the AuNPs synthesized using the citrate reduction method (PDI ≤ 0.177). UV–visible spectroscopic analysis showed a red-shift of the absorbance spectra after the reaction with MαHIgG$_4$, which indicated that the AuNPs were successfully conjugated. The optimum concentration of the *Bm*R1 recombinant antigen that was immobilized on the surface of the ICG strip on the test line was 1.0 mg ml^{-1}. When used with the ICG test strip assay and brugian filariasis serum samples, the conjugated AuNPs–MαHIgG$_4$ synthesized using the seeding-growth method had faster detection times, as compared with the AuNPs synthesized using the citrate reduction method. The 30 nm AuNPs–MαHIgG$_4$, with an optical density of 4 from the seeding-growth method, demonstrated the best performance for labelling ICG strips because it displayed the best sensitivity and the highest specificity when tested with serum samples from brugian filariasis patients and controls.

(Some figures may appear in colour only in the online journal)

1. Introduction

Gold nanoparticles (AuNPs) with sizes ranging from 10 to 100 nm have a large light absorption and scattering cross-section in the surface plasmon resonance (SPR) wavelength region. The magnitude of light scattering by AuNPs can be orders of magnitude higher than that of the light emission from strong fluorescence dyes [1]. This unique property has led to several important and promising applications of AuNPs in biomedical fields such as diagnostic

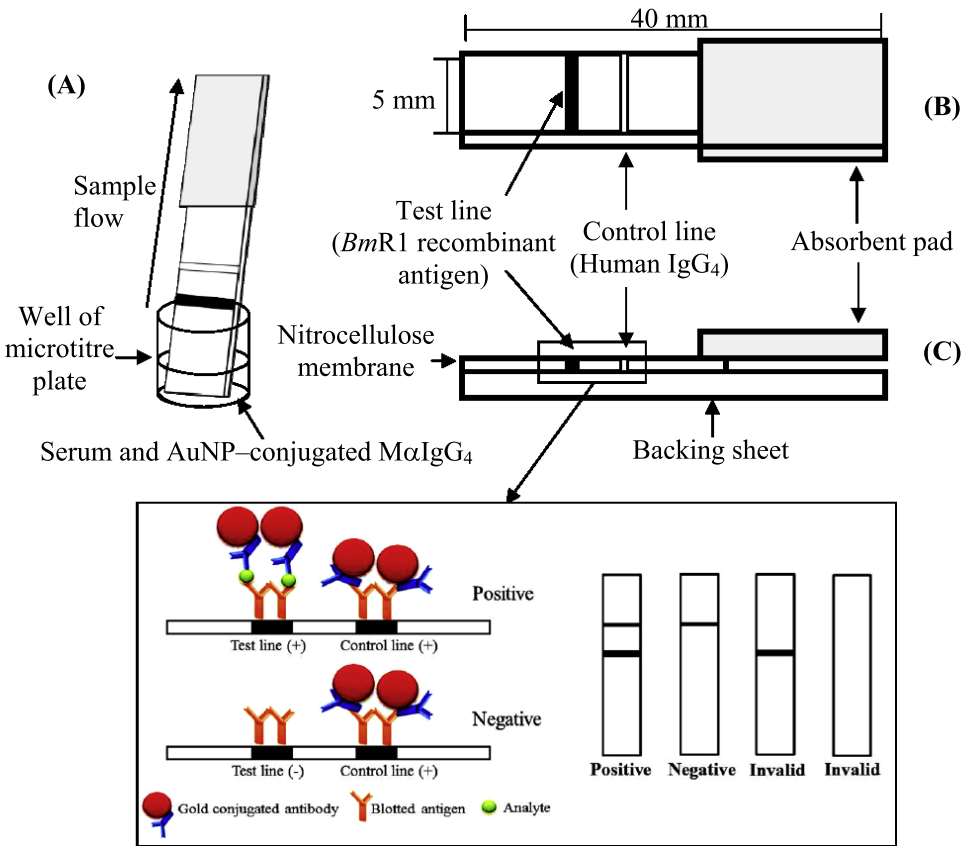

Figure 1. Schematic diagram of the working principle and structure of the ICG test strip. (A) The experimental set-up with (B) the top view and (C) the cross-section of the strip. the inset shows the sandwich format and interpretation of the ICG strip results.

and photo-thermal imaging, molecular and cancer cell biomarker visualization, and biosensing [2, 3]. AuNPs are excellent candidates for surface functionalization because they are easily synthesized, biocompatible, easily attached to molecules, and can be mobilized in biological systems [4, 5]. The ease of conjugating AuNPs with biomolecules and immobilizing them to a specific area makes AuNPs of interest for the preparation of biosensors for diagnostics [6].

The development of an immunoassay with a lateral flow test format that is based on immunochromatography for the diagnosis of specific diseases has gained much interest as a rapid point-of-care test which can be transported at room temperature [7]. The test results can be visually observed and easily interpreted, thereby allowing the diagnostic test to be performed in the field with the advantages of its sensitivity, specificity and user-friendly analysis [8]. Therefore, immunochromatographic (ICG) tests using AuNP-conjugated proteins such as the lateral flow diagnostic test are attractive tools for the development of biosensors [9, 10].

Generally, there are two main formats of the ICG strip assay, that is, the sandwich and competitive formats [8]. The competitive format is used more often to detect small molecules with a single antigenic determinant such as DNA. In the competitive format, free or unlabelled analytes in the sample block the binding sites of the antibodies and prevent the uptake of coloured particles. Thus, the response is negatively correlated to the concentration of the analyte. When more analytes are present, a low signal is obtained, whereas a high signal is obtained in the absence of an analyte [11]. Consequently, only the control line appears in a positive result, whereas both the test and control lines appear in a negative result. According to Zhang *et al* [8], the sandwich format is used to detect larger analytes with multiple binding sites such as viruses and antibodies. Therefore, in the sandwich format, two lines (test and control lines) appear on the ICG strip in a positive result, and only the control line appears in a negative result, with the line intensity directly proportional to the amount of analyte present in the sample [11].

The basic working principle of the ICG strip assay used in this study is based on the sandwich assay, as illustrated in figure 1. The analytical signals are observed after a specific interaction of the ligand and the analytes such as an antigen–antibody complex. This specific interaction occurs in the membrane by the capillary effect of the medium. One format of an antibody detection test has the antigen immobilized on the membrane while a secondary antibody is conjugated with the AuNPs [12]. The antibody in the sample binds with the immobilized antigen (test line), and this antigen–antibody complex then binds to the detector, an AuNP-conjugated secondary antibody. A control line could be composed of a polyclonal or monoclonal antibody that can bind with the AuNP-conjugated secondary antibody. The visualized red colour is caused by the accumulation of the

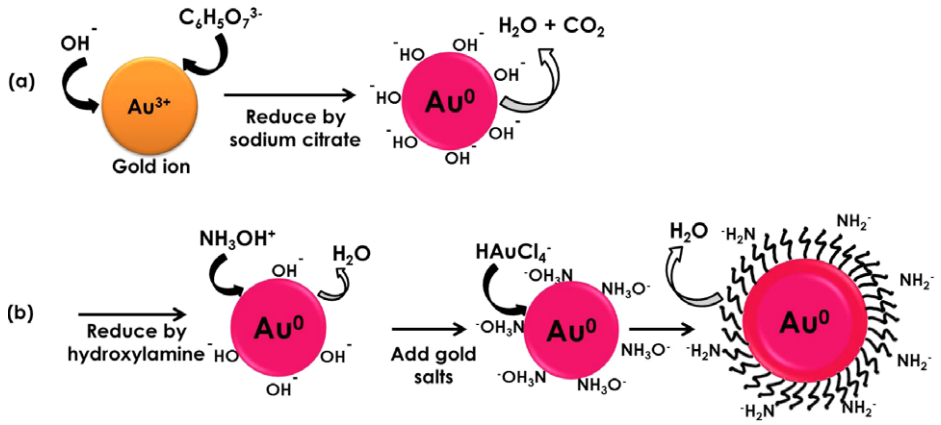

Figure 2. Schematic of AuNP formation during synthesis using (a) the citrate reduction and ((a) and (b)) the seeding-growth methods.

AuNPs at the locations of the test and control lines on the membrane [7, 9]. The intensity of the red colour on the test line is dependent on the concentration of the lined antigen (on the test line), the antibody in the sample, and the concentration of the colloidal AuNPs. Therefore, quantitative determination can be achieved by monitoring the intensity of the red colour that appears on the test line [13, 14].

A number of studies on the use of AuNPs in the ICG strip test have been reported. Most of the previous reports have used the well-known citrate reduction method for the synthesis of AuNPs with varying sizes, with trisodium citrate as the reducing agent [8, 10, 14–16]. In a typical citrate reduction, the reaction mechanism of AuNP formation is dependent on the concentration of the citrate ions ($C_6H_5O_7^{3-}$) and gold chloride ($HAuCl_4$) as well as the temperature during synthesis [17]. In this reduction reaction, the gold salt concentration, which is initially consumed for reduction by citrate ions ($C_6H_5O_7^{3-}$), becomes an important factor. The elaborate chemical reaction can be presented as

$$6Au^{3+} + C_6H_5O_7^{3-} + 15OH^- \rightarrow Au + 6CO_2 + 10H_2O. \quad (1)$$

The overall reaction mechanism of citrate reduction is illustrated in figure 2(a). After the said reaction, the AuNP surfaces are covered with the negatively charge surfactant (OH^-) that causes the particles to repel each other and remain stable in a colloidal form. Moreover, these OH^- ions with weak electrostatic charges are used as a medium of attraction during conjugation to the antibodies [18]. This method is facile; its major drawback is the tendency of the spherical gold particles to have an elliptical shape when the size exceeds 30 nm, which consequently produces polydispersed particles [19].

The seeding-growth method for the synthesis of AuNPs of various sizes was introduced by Brown and Natan [20] to overcome these drawbacks. The dimension and shape of the nanoparticles can be controlled, such that the size can be predetermined by allowing smaller particles to grow into larger particles using the seeding-growth method. The particles produced are more monodispersed as compared with the citrate reduction method. In this method, hydroxylamine (NH_2OH) plays a role as a reductant and prevents the formation of new nuclei by accelerating the reduction of Au^{3+} on the surface of the seeds, so that the growth process can occur [21, 22]. After all the seeds are covered by the NH_3O^- groups from hydroxylamine, the gold salts are added as a source of the Au^{3+} ions. These Au^{3+} ions are then diffused onto the surfaces of the seeds via a reaction with NH_3O^-, which causes the formation of larger sized AuNPs covered with NH_2^-, as illustrated in figures 2(a)–(b). The NH_2^- ions have an electrostatic charge and provide specific binding (amine bond) so that the AuNPs remain stable in the suspension [23]. The overall chemical reactions involved in the seeding-growth method are

$$\text{at the seed stage: } 6Au^{3+} + C_6H_5O_7^{3-} + 15OH^- \rightarrow 6Au + 6CO_2 + 10H_2O; \quad (2)$$

$$\text{at the growth stage: } Au + HAuCl_4^- + NH_3OH^+ \rightarrow 2Au + 4H_2O + 4Cl^- + NO. \quad (3)$$

To the best of the authors' knowledge, very few studies on protein labelling have used AuNPs that were synthesized using the seeding-growth method. In addition, the AuNPs produced using this method are readily available for conjugation with the protein through surface absorption and require a lower antibody concentration when applied to the ICG strip assay application as compared with the citrate reduction method. Moreover, the seeding-growth method allows for a specific interaction of the AuNP surfaces with the sites of the biomolecules through an ionic bond (NH_2^-). This binding improves the sensitivity of the conjugated AuNPs as detectors for labelling in the ICG strip assay.

The novelty of this work lies in the conjugation of AuNPs that were synthesized using the seeding-growth method to antibodies, as well as the properties of these conjugates as compared with the well-known citrate reduction method. The 20, 30 and 40 nm AuNPs were synthesized using both methods, conjugated with mouse anti-human IgG_4 ($M\alpha HIgG_4$), and then tested with the ICG strip test, which used the human IgG_4 antibody as the control line and a *Brugia malayi* recombinant protein (B*mR*1) as the test line. The effects of the AuNP size on the ease of conjugation,

sensitivity and efficiency were systematically studied. This process involves the binding of the recombinant antigen to the filarial-specific human IgG_4 antibodies in the serum samples of patients with brugian filariasis, followed by binding of the antigen–antibody complex to the AuNP-conjugated MαHIgG_4. The appearance of two lines (control and test lines) indicated a positive result, whereas the appearance of one line (control line) indicated a negative result. MαHIgG_4 was chosen because of its high sensitivity and specificity in detecting brugian filariasis. This disease is caused by a worm and transmitted by mosquitoes, which can lead to acute and chronic manifestations including fever, lymphatic inflammation and various degrees of leg enlargement [24, 25]. Brugian filariasis is a neglected tropical disease in developing countries. Thus, the results of this study are of practical importance to help reduce the price of diagnostic kits for resource-poor areas, aside from benefitting the lateral flow test industry in general.

To date, most diagnostic kits use 40 nm AuNPs but our study proved that 30 nm is the optimum size for use in the lateral flow immunoassay. The cost of the antibody in this immunoassay accounts for 80% of its total cost. In this study, we have shown that the AuNPs that were produced using the seeding-growth technique required fewer antibodies (∼50% less) than the AuNPs produced using the citrate reduction method. Thus, our proposed method will significantly reduce the production cost.

2. Materials and methods

2.1. Materials and reagents

Gold (III) chloride trihydrate ($HAuCl_4{\cdot}3H_2O$, Cat. # 520918), sodium citrate tribasic dehydrate ($Na_3C_6H_5O_7{\cdot}2H_2O$, Cat. # S4641), phosphate buffer solution (PBS, Cat. # P3619), bovine serum albumin (BSA, Cat. # A3803), HCl, HNO_3 and potassium carbonate (K_2CO_3, Cat. # 590681) were purchased from Sigma. Hydroxylamine hydrochloride ($NH_2OH{\cdot}HCl$, Cat. # 822334) was bought from Merck. Sodium chloride (NaCl, Cat. # X190) was bought from Solon, Ohio. Monoclonal mouse anti-human IgG_4 (Cat. # A10651) was purchased from Invitrogen and human IgG_4 (Cat. # 400126) was purchased from Calbiochem, Merck. The B*mR*1 recombinant antigen and the human serum samples were provided by one of the authors; the latter were obtained in accordance with the requirements of the Universiti Sains Malaysia (USM) Human Research Ethics Committee. The blocking solution (Cat. # 11921673001) was purchased from Roche Diagnostics and Tris-HCl (Cat. # T3253) was purchased from Sigma. Hi-flow Plus 90 Membrane Cards (60 mm × 301 mm) were purchased from Millipore, whereas the absorbance pad (grade 222) was purchased from Schleicher & Schuell.

2.2. Instrumentation and apparatus

The AuNP particle sizes were examined by transmission electron microscopy (TEM) and analysed using the FEI CM12 (version 3.L) image analysis system at 120 kV. The particle size distribution was measured from several TEM images by counting 300 nanoparticles using ImageJ software. The dispersity of the AuNPs after synthesis was characterized using a Zetasizer particle electrophoresis instrument (Nanoseries Model ZEN3600, Malvern Instruments). The absorbance properties of the AuNPs before and after conjugation were determined using a UV–vis–NIR spectrophotometer (Model UV-3600, Shimadzu). An IsoFlow dispenser (Imagene Technology) was used to prepare the test and control lines on nitrocellulose (NC) membrane cards. All glassware was cleaned in a bath containing freshly prepared aqua regia ($HCl{:}HNO_3$, 3:1, v/v) and rinsed well with ultrapure water. Ultrapure Millipore water from a Milli-Q system (18.2 MΩ cm at 25 °C) was used during the synthesis.

2.3. Synthesis of AuNPs using the citrate reduction method

AuNPs with particle sizes of 20, 30 and 40 nm were synthesized using a typical citrate reduction method [15, 16, 26]. Briefly, 0.01% (w/v) $HAuCl_4{\cdot}3H_2O$ was prepared in an Erlenmeyer flask, stirred and heated to boiling. Then, 1% (w/v) trisodium citrate was immediately added. The solution was boiled to ensure a complete reaction. The amount of trisodium citrate added was adjusted to 2, 1.4 and 1 ml to produce 20, 30 and 40 nm colloidal AuNPs, respectively. After 30 s of trisodium citrate addition, the colour of the solution changed from light yellow to faint blue, which indicated that the nucleation process had occurred. Then, the colour changed to grey-blue before finally becoming a dark red colour, which indicated the formation of spherical particles. The reduction process was completed when the colour changed completely from grey-blue to burgundy red wine colour. The AuNP solution was stirred continuously then cooled to room temperature. The obtained suspension was stored at 4 °C.

2.4. Synthesis of AuNPs via the seeding-growth method

Colloidal AuNPs with particle sizes of 20, 30 and 40 nm were prepared using the modified seeding-growth method [27]. This method is composed of two stages: gold seeds are prepared in the first stage, which is followed by the growth process in the second stage. Larger particles were produced by the reduction of $HAuCl_4$ with hydroxylamine amine as a mild reducing agent in the presence of existing AuNP seeds. Therefore, hydroxylamine hydrochloride functions as a growth agent, as opposed to a nucleation agent, in slightly acidic conditions [28]. AuNP seeds with 15 nm diameters were then grown to sizes of 20, 30 and 40 nm by consecutively varying the volume of the seed solution. The preparation of this seed solution is similar to the typical citrate reduction method [26]. At the growth stage, a certain volume of freshly prepared seed solution (4, 7 and 10 ml) was added into $NH_2OH{\cdot}HCl$ while stirring. Finally, gold chloride was added dropwise with continuous stirring. The reduction process was completed within 5 min.

2.5. Conjugation of mouse anti-human IgG$_4$ to AuNPs (AuNPs–MαHIgG$_4$)

The pH of the colloidal AuNPs was adjusted to a value that was slightly higher than the isoelectric point (IEP) of the antibody. For MαHIgG$_4$, the IEP value was approximately 5.5–6. Therefore, the pH of the AuNPs was adjusted to 7 by adding 0.2 M K_2CO_3. The optimum concentration of MαHIgG$_4$ for stabilizing AuNPs was determined by adding a constant volume (e.g., 500 μl) of each of the pH-adjusted AuNPs with varying sizes (20, 30 and 40 nm) to a serial dilution of MαHIgG$_4$ (e.g., 1, 3, 6, 8 and 12 μg ml^{-1}) tubes. After incubating at room temperature for 15 min, the tubes were vortexed, and 500 μl of 10% NaCl was added. At this step, flocculation occurred because of the presence of high salt concentrations. The optimum concentration of protein (MαHIgG$_4$) that was required to stabilize the AuNPs was chosen by observing the lowest concentration of MαHIgG$_4$ that did not change colour after 10% NaCl was added [29, 30]. All the AuNP solutions had an optical density (OD) close to 1. The optimized concentration of MαHIgG$_4$ was then added to 1 ml of the pH-adjusted AuNPs. The solution was gently mixed and incubated for 30 min at room temperature. BSA (1%) in Millipore water was added to the solution to stabilize the mixture. The excess unconjugated MαHIgG$_4$ was removed, and the remaining unbound sites on the AuNP surfaces were blocked. After vortexing, the solution was centrifuged at 10 000 rpm (7378*g*) for 10 min. This washing step was repeated twice because the excess antibodies competed with the AuNPs–MαHIgG$_4$ in the subsequent assay. After the supernatant was removed, the pellet was resuspended in 1% BSA and stored at 4 °C.

2.6. ICG dipstick and assay procedure

The *Bm*R1 recombinant antigen, as a test line, and the human IgG$_4$, as a control line, were prepared on an HF 90 NC membrane using an IsoFlow dispenser at a dispenser rate of 0.1 μl mm^{-1}. The NC membrane was chosen because of its high protein binding capacity (primary electrostatic binding) and its hydrophobic property. The conjugated antibodies similarly have hydrophobic characteristics; consequently, they could interact with the NC and can be effectively dried onto the membrane [31]. For the *Bm*R1 recombinant antigen, the line was dispensed at concentrations of 0.75, 1.0 and 1.5 mg ml^{-1}, whereas the control antibody line was dispensed at 0.7 mg ml^{-1}. After the lining, the NC membrane was dried in an oven at 37 °C for 2 h. Then, the remaining protein binding sites on the NC membrane were immersed in a blocking solution containing 10% casein, Tris-HCl and 0.01 M TBS at pH 7.5. In addition, the blocking solution allowed proteins to flow through the ICG strip without any residues [32]. After overnight drying at 37 °C, the NC membrane was cut (5 mm/strip), and an absorbent pad was attached to the backing sheet at the top of the NC, with a 2 mm area overlapping the membrane. The layout of the test strips with the ICG schematic and test format is shown in figure 1. The strips were then sealed and stored in a desiccator that maintained a relative humidity of less than 20%.

For the sample analysis, a positive serum sample from a patient with brugian filariasis was diluted with an equal volume of PBS (pH 7.2) in a well of a microtitre plate (figure 1). The strip was then placed in the well and the timer was started. After 3 min, the colloidal AuNPs conjugated to MαHIgG$_4$ were added into the well and allowed to flow until the conjugated AuNPs exceeded the control line on the strip. The strip was then washed with PBS buffer to remove any unspecific interactions and background colours. The performances of the 20, 30 and 40 nm colloidal AuNPs that were synthesized using the citrate reduction and seeding-growth methods, each of which were conjugated to MαHIgG$_4$, were compared in terms of the detection time and the colour intensity of the control and test lines. The colour intensity for the signal was converted to a grey-scale reading and quantified using ImageJ software. The sensitivities of the 30 and 40 nm AuNPs from the seeding-growth technique were then tested with a series of diluted positive sera (dilution performed with the serum sample of a healthy individual) starting from a neat (undiluted) serum sample, followed by dilutions of 1:2, 1:4, 1:8, 1:16, 1:32, 1:64, 1:128 and 1: 256. The neat serum had an optical density (OD) of 3, as measured using an ELISA reader at a wavelength of 280 nm. The 30 nm AuNPs of varying ODs (OD: 8, 7, 6, 5, 4, 3, 2, 1) from the seeding-growth method were then tested to identify the OD that produced the clearest test and control lines on the ICG strip with the most dilute positive serum sample. The specificity testing was performed with the optimized OD of the 30 nm AuNPs using low and high positive serum samples from patients with brugian filariasis and negative (control) serum samples. The latter were composed of samples from patients with other parasitic infections, namely, roundworm (*Ascaris lumbricoides*), whipworm (*Trichuris trichiura*) and amoebiasis (*Entamoeba histolytica*). The analysis was repeated three times to prove the repeatability of the analysis.

3. Results and discussion

3.1. Characterization of the colloidal AuNPs

Colloidal AuNPs were successfully synthesized using the citrate reduction and seeding-growth methods. The TEM images of colloidal AuNPs that were synthesized using both methods have a well-dispersed distribution of AuNPs, as shown in figures 3 and 4(a)–(c). The particle size distribution of the AuNPs from the TEM images was measured using ImageJ software and represented in the histograms, as shown in figures 3(d)–(f) for the citrate reduction method and figures 4(d)–(f) for the seeding-growth method. The TEM analysis showed that the diameters for each of the AuNP sizes (20, 30 and 40 nm) were almost uniform. The ellipticity of the nanoparticles was determined from calculations of the major and minor axes. The major axis refers to the longest diameter of the nanoparticles, whereas the minor axis refers to the shortest diameter of the nanoparticles. The ellipticity of the nanoparticle (G) is defined as the ratio between the major and minor axes; this ratio should be 1 if it is

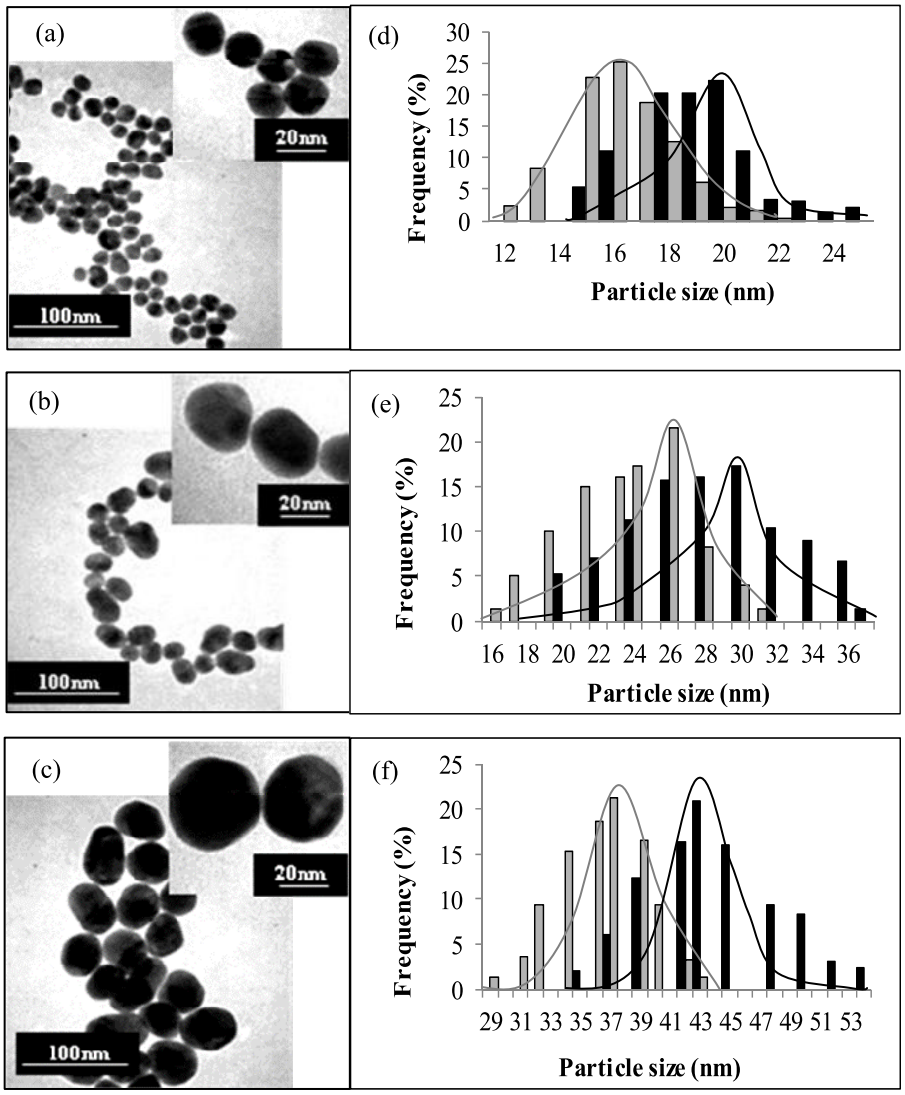

Figure 3. TEM images of the (a) 20 nm, (b) 30 nm and (c) 40 nm AuNPs produced using the citrate reduction method with the corresponding particle size histograms in (d)–(f), respectively. Black and grey lines represent the major axis (long direction) and the minor axis (short direction), respectively.

Table 1. AuNP sizes of samples obtained from the citrate reduction and seeding-growth methods.

	Citrate reduction method				Seeding-growth method			
Size of AuNPs (nm)	Major axis (nm)	Minor axis (nm)	Ellipticity (G)	Standard deviation (σ)	Major axis (nm)	Minor axis (nm)	Ellipticity (G)	Standard deviation (σ)
20	19	16	1.18	2.04	24	23	1.02	1.80
30	30	26	1.15	4.34	32	31	1.03	3.08
40	43	37	1.16	4.31	40	36	1.11	3.64

circular (2D projection of a spherical particle) [23]. Haiss *et al* [33] described particles as spherical when the ratio of the long to short axis was between 1.05 and 1.25. In this study, the ellipticities of the 20, 30 and 40 nm AuNPs that were produced using the seeding-growth method were 1.02, 1.03 and 1.11, as compared with the results of the citrate reduction method of 1.18, 1.15 and 1.16, respectively, as listed in table 1. However, all the produced AuNPs could be considered as spherical with a low G ($\leq$1.18) [33]. Compared with the citrate reduction method, the seeding-growth method produced more homogeneous spherical AuNPs than those without non-spherical structures. Moreover, the AuNPs that were synthesized using the seeding-growth method showed lower G values ($\leq$1.11) as compared with previous research that used the seeding-growth approach, with $G \leq 1.13$ [23]. The homogeneity of the particle size distribution of the synthesized AuNPs is represented by the standard deviation (σ) that was measured from the TEM images (table 1).

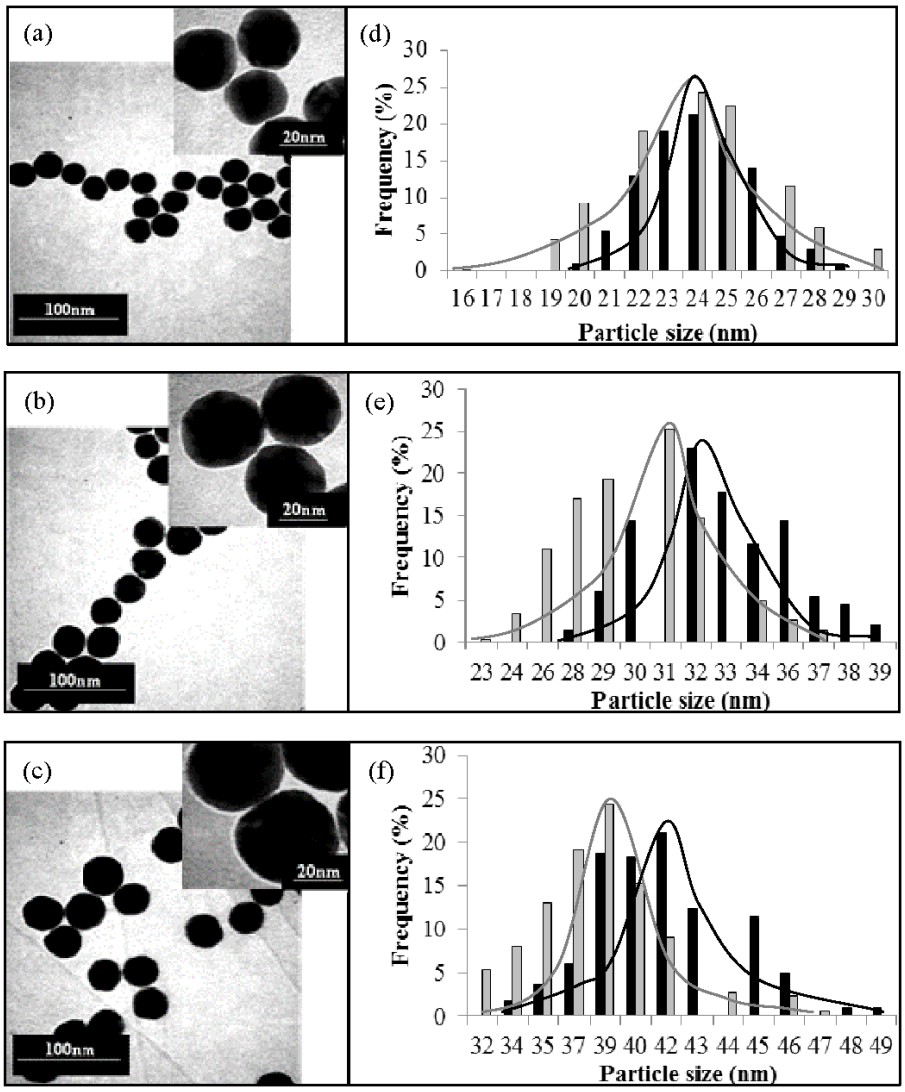

Figure 4. TEM images of the (a) 20 nm, (b) 30 nm and (c) 40 nm AuNPs produced using the seeding-growth method, with the corresponding size histograms in (d)–(f), respectively. Black and grey lines represent the major axis (long direction) and the minor axis (short direction), respectively.

The σ values for the 20, 30 and 40 nm AuNPs that were synthesized using the seeding-growth method showed smaller values (1.80, 3.08 and 3.64, respectively) as compared with the AuNPs synthesized using the citrate reduction method (2.04, 4.34 and 4.31, respectively). This analysis indicates that the AuNPs synthesized using the seeding-growth method have a small range of particle size distribution as compared with the AuNPs that were synthesized using the citrate reduction method. Baptista *et al* [34] found that the successful utilization of AuNPs in biological assays, especially in the ICG strip, relies on the availability of the synthetic methods to generate high-quality AuNPs. A high-quality AuNP is defined as a particle that has the desired characteristics, namely, high solubility in water, homogeneity in morphology and size dispersion, as well as good surface functionalities [34, 35]. The uniformity of particle size is important to control the load of AuNPs attached to the antibody for conjugation purposes. In addition, the stability of colloidal AuNPs in solution is an indicator of high-quality AuNPs [11]. A stable suspension ensures a uniform distribution of the conjugates during its application in the ICG strip assay.

In the citrate reduction method, trisodium citrate was used as a reducing agent to reduce the gold chloride ions to AuNPs. When the amount of trisodium citrate was reduced, the size of the AuNPs was increased. Volumes of 2, 1.4 and 1 ml of 1% (w/v) trisodium citrate produced 20, 30 and 40 nm nanoparticles, respectively. Supersaturation of the solution with respect to gold formation only occurred when $AuCl_4^-$ was formed during the nucleation process. The degree of supersaturation is controlled by the number of nuclei formed by the reduction reaction of citrate ions, as in equation (1). If a higher concentration of citrate ions is present in the solution, more nuclei are formed, which causes faster supersaturation and forms smaller AuNPs. If fewer citrate ions are present in the solution, the formation of nuclei occurs at a slower rate. The slow chemical reduction causes their deposition to sites of the lowest free energy, which aids facet development [17, 36, 37]. Therefore, a degree of supersaturation could be

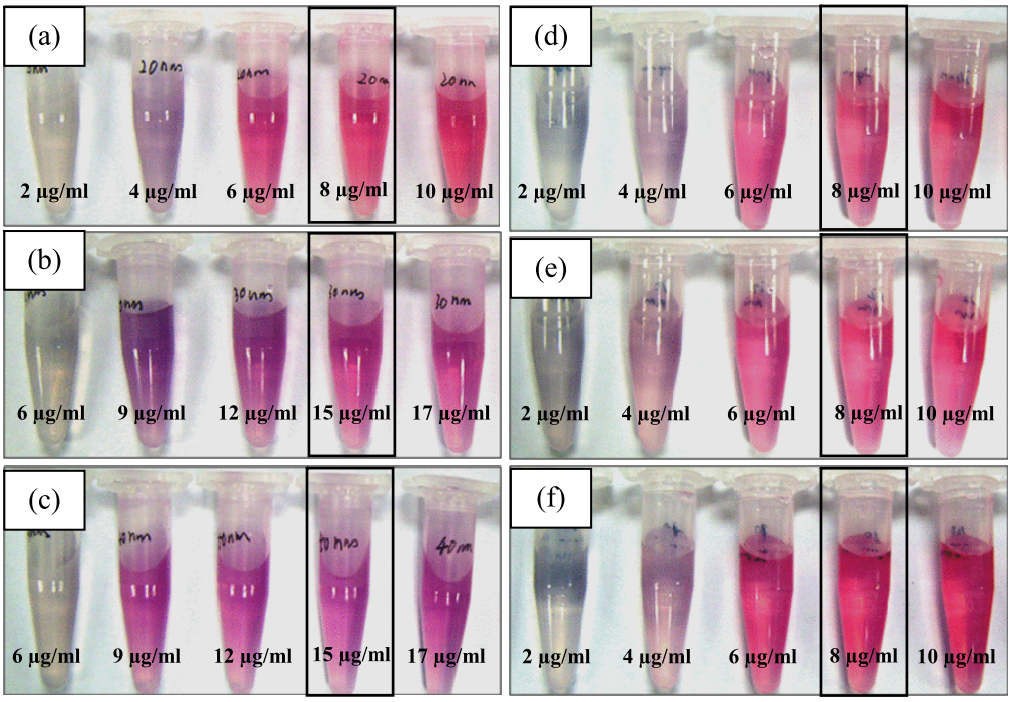

Figure 5. Concentration gradients of AuNPs–MαHIgG$_4$ mixtures after incubation. The three tubes on the left contain insufficient amounts of MαHIgG$_4$ to stabilize the AuNPs when 10% NaCl is added. The fourth tube has the optimum concentration of MαHIgG$_4$ to stabilize the AuNPs, as labelled in the diagrams. The fifth tube contains excess MαHIgG$_4$. The 20, 30 and 40 nm AuNPs produced using the citrate reduction and seeding-growth methods are labelled as (a)–(c) and (d)–(f), respectively.

achieved over a longer period to cause the formation of non-homogeneous and elliptical structure as in figures 3(b) and (c).

In the seeding-growth method, the formation mechanism of the seed nanoparticles at the seed stage is similar to the citrate reduction method. In the growth stage, $NH_2OH{\cdot}HCl$ was introduced as a reducing agent that modified the surface of the seed nanoparticles. The seeds served as nucleation centres so that all the gold ions were diffused on the seeds' surfaces to enlarge the AuNPs [38]. NH_2OH served as a mild reducing agent, which reduced the gold salts into AuNPs, where reactions only occurred at room temperature. The full mechanisms are illustrated in figure 2 and simplified in equations (2) and (3). As shown in figure 4, all the AuNPs obtained by this method are spherical and homogenous in size (with a very low standard deviation as compared with the citrate reduction method, table 1). This result shows that the 0.1 M NH_2OH used in this synthesis was sufficient to cap the Au seeds as well as to cause the reduction and diffusion of the Au ions to occur only on the surfaces of the seeds without new nucleation.

3.2. Characterization of the AuNP-conjugated antibody

In the conjugation step, the most important factor is to control the pH of both the antibody and the colloidal gold. The AuNPs that were prepared using the citrate reduction and seeding-growth methods consisted of negative ionic double layers of charges surrounding the Au core; these electrostatic charges prevented the AuNPs from aggregating. When NaCl was added into the AuNP solution, the double layer was destroyed, and the AuNPs had a tendency to aggregate. Therefore, the steric repulsion and screening property of the AuNPs from the ionic interaction would not be affected and destroyed by NaCl in the presence of sufficient antibodies to cover the surfaces of the AuNPs [36].

The minimum amount of antibodies required to stabilize the colloidal AuNPs was selected by considering the minimum amount of MαHIgG$_4$ that could prevent flocculation (without changing the red colour of the AuNPs) [39]. The concentration gradient to stabilize the AuNPs is shown in figures 5(a)–(c) for the AuNPs that were produced using the citrate reduction method and figures 5(d)–(f) for those synthesized using the seeding-growth method. The required MαHIgG$_4$ to stabilize the AuNPs synthesized using the citrate reduction method was higher (8, 15 and 15 μg ml^{-1} for 20, 30 and 40 nm, respectively) as compared with the seeding-growth method (8 μg ml^{-1} each for 20, 30 and 40 nm, respectively); this is shown in the fourth tube in figure 5. The higher requirement is caused by the type of ionic charges that surround the AuNP surface, which cause electrostatic interaction and absorb MαHIgG$_4$ on the AuNP surface at a specific IEP [18, 40, 41]. Similarly to figure 2, the AuNPs from the citrate reduction method were covered by an ionic double layer of OH^- ions. These charges caused random absorption of MαHIgG$_4$ onto the AuNP surface. On the other hand, AuNPs synthesized using the seeding-growth method contained the amine group (NH_2^-) on the surface. These NH_2^- ions provided a specific interaction such that MαHIgG$_4$ could be absorbed at

Table 2. UV–vis absorption spectra of AuNPs which were synthesized using the citrate reduction and seeding-growth methods before and after conjugation with MαHIgG$_4$.

Synthesis method	Before conjugation				After conjugation			
	Citrate reduction		Seeding-growth		Citrate reduction		Seeding-growth	
Size of AuNPs (nm)	λ_{max} (nm)	Abs. (OD)	λ_{max} (nm)	Abs. (OD)	λ_{max}(nm)	Abs. (OD)	λ_{max}(nm)	Abs. (OD)
20	519	0.942	521	0.938	528	10	527	10
30	527	0.961	523	1.003	536	10	528	10
40	528	1.056	525	1.067	540	10	530	10

a specific bridge provided by the amine bond. Therefore, the seeding-growth method required less MαHIgG$_4$ to stabilize the AuNP surface.

The absorption spectra of the AuNPs before and after conjugation with MαHIgG$_4$ are summarized in table 2. For the 20, 30 and 40 nm AuNPs synthesized using the citrate reduction method, surface plasmon absorption occurred at 519, 527 and 528 nm respectively. Meanwhile, the absorption spectra of the 20, 30 and 40 nm AuNPs produced via the seeding-growth method were obtained at 521, 523 and 525 nm, respectively, as shown in table 2. The SPR frequency of AuNPs depends on several factors such as the particle size, shape, aggregate morphology, ligands, medium dielectric property and refractive index of the surrounding medium [42, 43]. According to Norman *et al* [44], small shifts in the position of the SPR occur as a result of changes in the dielectric properties of the AuNP medium or the presence of materials adsorbed on the surfaces of the AuNPs. Therefore, although the AuNPs had similar sizes, their measurement peaks were different when using different synthesis methods because of the interference that occurred on the surfaces of the AuNPs. The surface charge of AuNPs synthesized using the citrate reduction method is OH^- and for the seeding-growth method it is NH_2^-. Hence, the peak deviates slightly to the right for the seeding-growth method because of the presence of amine molecules on the surface. In addition, the AuNPs synthesized using the seeding-growth method showed lower polydispersity index (PDI) values as compared with the AuNPs synthesized using the citrate reduction method (figure 6). Although the PDI value was small, increasing the size of the AuNPs made this PDI effect become more significant, whereby the peak spectra were determined by scattering rather than absorption, which is in agreement with the study of Ziegler and Eychmüller [45]. The surface plasmon absorption of AuNPs also showed a size dependence indicated by a red-shift with a broader band of the peak wavelength as the size of AuNPs increased. This dependence is due to the effect of the intense colour of AuNPs, which is attributed to the collective oscillation of the free conduction electrons. The free conduction electrons in the surface plasmon resonate with the incident photon frequency and cause the specific absorbance in a visible range [46, 47]. The presence of single absorption spectra as summarized in table 2 shows that only spherical AuNPs were produced using both methods. UV–vis absorption spectra were not only used to measure the mean size of the AuNPs but also to evaluate their polydispersity, which is in agreement with

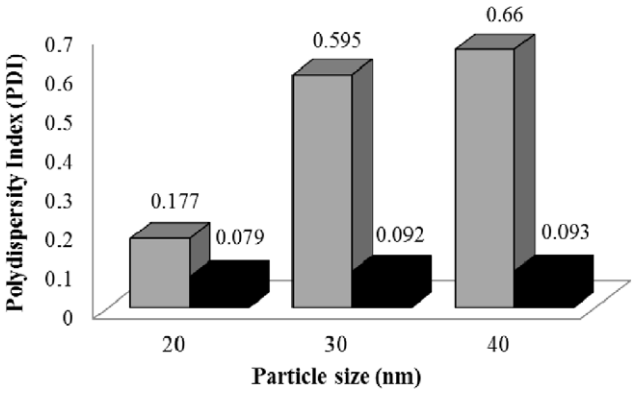

Figure 6. PDIs of AuNPs with varying sizes. The black and grey areas represent AuNPs synthesized using the seeding-growth and citrate reduction methods, respectively.

Bogatyrev *et al* [48]. Their work studied the mean size and the evaluation of polydispersity of AuNPs using optical absorption and scattering spectra. Their group suggested that when the extinction spectra are virtually identical, the scattering spectra show a pronounced increase in the peak amplitude, whereby the polydispersity of colloidal AuNPs can be simulated and confirmed with calculations based on the Mie theory.

The SPRs of the 20, 30 and 40 nm AuNPs using the citrate reduction method conjugated MαHIgG$_4$ show that the maximum peaks were observed at 528, 536 and 540 nm (table 2), respectively, because of the surface resonance interactions with the antibody. The maximum peaks for 20, 30 and 40 nm AuNPs–MαHIgG$_4$ from the seeding-growth method were observed at 527, 528 and 530 nm (table 2), respectively. By comparing the UV–vis absorption spectra for AuNPs synthesized using the citrate reduction and seeding-growth methods before and after conjugation with MαHIgG$_4$, the results showed that the surface resonance band shifted to the red (right) after the conjugation process. The red-shift in the plasmon peak for all samples proved that all AuNPs were successfully conjugated to MαHIgG$_4$. This red-shift was due to the changes in the local refractive index after the addition of the protein layer around the nanoparticles [18]. This analysis proved that the produced AuNPs–MαHIgG$_4$ was stable and not aggregated because of the absence of a strong red-shift in the absorbance, as observed in table 2.

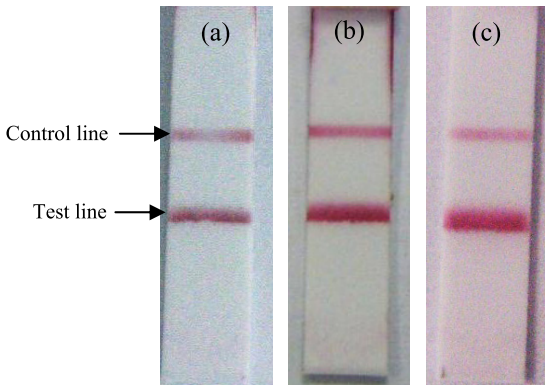

Figure 7. AuNPs–MαHIgG$_4$-labelled ICG strips with varying test line (*Bm*R1 recombinant antigen) concentrations: (a) 0.75 mg ml^{-1}, (b) 1.0 mg ml^{-1} and (c) 1.5 mg ml^{-1}.

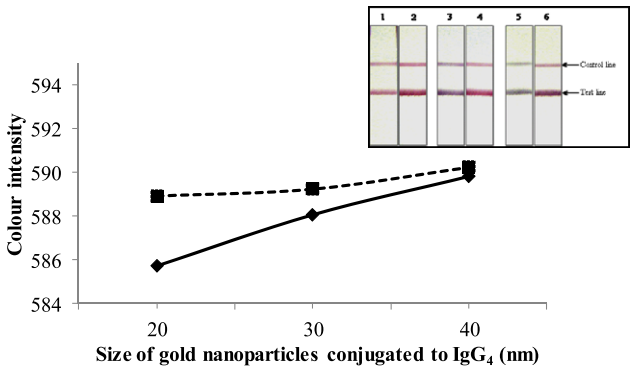

Figure 8. Dependence of the colour intensity on the varying sizes of the AuNPs–MαHIgG$_4$ on the test line of the developed ICG test strip in the inset. (Results of testing with positive serum samples using ICG strips containing different sizes of AuNPs–MαHIgG$_4$.) The solid and dashed lines represent AuNPs produced using the citrate reduction and seeding-growth methods, respectively. The intensity values were measured using ImageJ software.

3.3. Sensitivity and specificity performance of the ICG strip assay

First, the concentration of the *Bm*R1 recombinant antigen, which was immobilized as the test line on the ICG strip, was optimized at 1.0 mg ml^{-1} based on the equally intense appearance of both the test and control lines (figure 7(b)). With 0.75 mg ml^{-1} of the *Bm*R1 antigen (figure 7(a)), the test line showed low and unacceptable intensity. On the other hand, at 1.5 mg ml^{-1} *Bm*R1 antigen (figure 7(c)), a broad test line was observed, and this caused the control line to appear much less intense.

The obtained ICG test strip results with different sizes of AuNPs–MαHIgG$_4$ are shown in the insets of figures 8 and 9. The 20, 30 and 40 nm AuNPs that were produced using the seeding-growth method and conjugated to MαHIgG$_4$ allowed for good visualization of target molecules on the NC membrane as compared with the AuNPs synthesized using the citrate reduction method. After the analysis of each ICG strip using ImageJ software, higher colour intensities of the lines using larger AuNP particle sizes (40 nm) conjugated to MαHIgG$_4$, which were synthesized using both methods, were observed as compared with the smaller AuNPs. The results show that when the size of the AuNPs increases, the visibility of the lines on the ICG strip assay consequently increases because of the natural optical properties of AuNPs; these nanoparticles have more vivid colours when their sizes become larger [49, 50]. This result shows why 40 nm AuNPs are commonly used in manufacturing diagnostic kits [35, 49, 51]. However, by comparing the colour intensities from the synthesis point of view, the 20, 30 and 40 nm AuNPs synthesized using the seeding-growth method showed better colour intensities when conjugated to MαHIgG$_4$ as compared with those synthesized using the citrate reduction method (figure 8). In this observation, the surface ionic charges of the AuNPs greatly influence the conjugation behaviour and its labelling properties on the ICG strip. NH_2^-, as the surface ionic charges for AuNPs synthesized using the seeding-growth method (figure 2(b)), have specific amine bonds with MαHIgG$_4$. This specific bridging provides a strong binding affinity to gold conjugation. On the other hand,

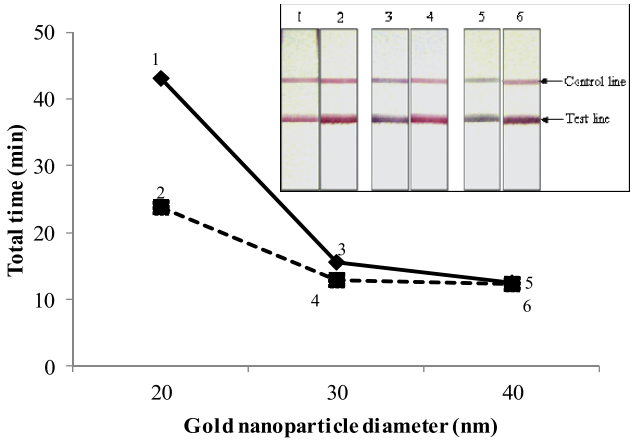

Figure 9. Total time performance of the ICG test strip tested with positive serum (from the inset figure). The solid and dashed lines represent AuNPs produced using the citrate reduction and seeding-growth methods, respectively.

the ionic charges (OH$^-$) capped on the surface of AuNPs that were synthesized using the citrate reduction method (figure 2(a)) randomly attract the MαHIgG$_4$ molecules but have a weak binding affinity. Thus, the AuNP-conjugated MαHIgG$_4$ from the seeding-growth method has a better binding affinity and produces larger signals on the labelling ICG strip as compared with the conjugated AuNPs from the citrate reduction method.

The detection time using AuNPs–MαHIgG$_4$ that was produced via both methods is demonstrated in figure 9. From the graph, the 40 nm AuNPs–MαHIgG$_4$ from both methods showed the fastest detection time (12 min) and the 20 nm AuNPs–IgG$_4$ showed the slowest detection time (23 min). The HF 90 type NC membrane consists of various pore sizes with large porosity; thus, the mobility of the particles could be restricted depending on the size of the AuNPs and the viscosity of the antigen [52]. The larger AuNPs–MαHIgG$_4$ flows faster by flowing only through the larger pores as compared with the smaller AuNPs–MαHIgG$_4$

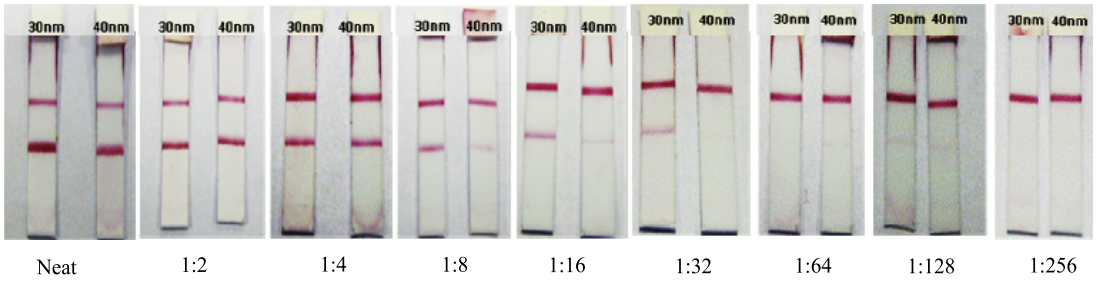

Figure 10. Comparison of the sensitivities of the 30 and 40 nm AuNPs–MαHIgG$_4$ on ICG strips for detecting antibodies in increasing dilutions of a positive serum sample.

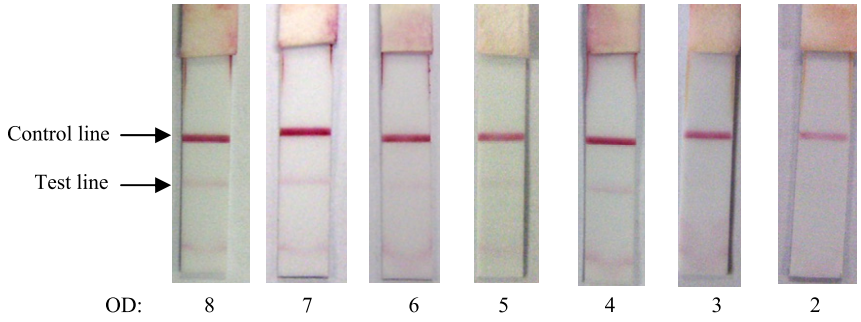

Figure 11. The ICG strip of the 30 nm AuNPs–MαHIgG$_4$ with varying OD, which was tested with positive serum at 1:128 dilution.

particles that flow through the small pores. Hence, the smaller AuNPs–MαHIgG$_4$ requires a longer detection time on an ICG strip.

The 30 nm AuNPs–MαHIgG$_4$ detected the antibodies at a higher serum dilution of 1:128 as compared with that of 40 nm AuNPs–MαHIgG$_4$, which detected antibodies at a lower serum dilution of 1:32 (figure 10). This observation can be attributed to the capacity of the 30 nm AuNPs–MαHIgG$_4$ to pass more easily through to the small pores of the NC membrane as compared with the 40 nm AuNPs–MαHIgG$_4$. Thus, the sensitivity is enhanced. The OD of 30 nm AuNPs–MαHIgG$_4$ was then varied to 8, 7, 6, 5, 4, 3 and 2. These varied conjugates were tested on the ICG strip (figure 11). The lowest OD of the 30 nm AuNPs–MαHIgG$_4$ at the serum dilution of 1:128 was determined to be 4, for which the test line on the ICG strip is still clearly visible to the naked eye. The test line was not observed with OD 2–3 because of the presence of a very low amount of AuNPs–MαHIgG$_4$. This observation suggests that OD 4 is the lowest OD that should be used in further studies to minimize the cost. Specificity testing of the 30 nm AuNPs–MαHIgG$_4$ was then performed on several types of human serum samples. The ICG strips showed two visible lines (positive results) with low positive serum (LPS) and high positive serum (HPS) samples from brugian filariasis patients. On the other hand, only the control line appeared (negative results) on the strip when tested with the negative (control) serum sample. Thus, the result showed that the 30 nm AuNPs–MαHIgG$_4$ was specifically bound to the specific antigen (*Bm*R1)–antibody complex at the test line and to the antibody at the control line (figure 12(a)). This study showed that the smaller AuNPs possessed the best labelling efficiency (ability of the gold-conjugated antibody to effectively detect the presence of an analyte from the serum on the detection zone), whereas the larger nanoparticles possessed the best sensitivity as a detector on the ICG strip assay. Similar results have been obtained by other researchers [7, 31, 50]. Kaur *et al* [7] studied the sensitivity enhancement of a dipstick with gold particles labelled with hapten–protein conjugates bound to antibodies on the NC strips using an enhancer—a mixture of gold chloride and hydroxylamine. They concluded that larger Au nanoparticles are beneficial for the visualization or quantification of the target molecules on an NC membrane used in dipstick immunoassays. However, small AuNPs are usually used to prepare the conjugate to increase the labelling efficiency. In addition, Bergen en Henegouwen and Leunissen [29, 53] demonstrated that the labelling efficiency decreases dramatically with increasing particle size because of bad penetration, steric hindrance and/or repulsion forces of gold conjugates.

4. Conclusion

AuNPs with sizes of 20, 30 and 40 nm were successfully produced using the citrate reduction and seeding-growth methods. MαHIgG$_4$ was successfully conjugated to all sizes of AuNPs, as confirmed by UV–vis analysis. The 20, 30 and 40 nm AuNPs produced using the seeding-growth method conjugated to MαHIgG$_4$ showed faster detection time compared with the AuNPs synthesized using the citrate reduction method on ICG strip assay when tested with serum samples from patients with brugian filariasis. The 30 and 40 nm AuNPs–MαHIgG$_4$ had a detection time of less than 15 min, but the 30 nm AuNPs–MαHIgG$_4$ showed the highest sensitivity level when tested with serum samples

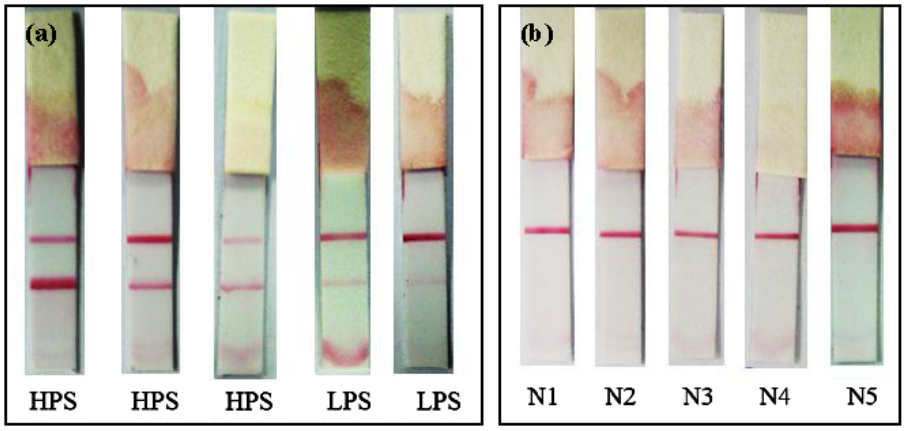

Figure 12. The ICG strip of the 30 nm AuNPs–MαHIgG$_4$ at OD 4 tested with different types of serum samples. (a) HPS and LPS serum samples from brugian filariasis patients. (b) Negative (control) serum samples: N1 and N2, from patients with mixed roundworm infections, i.e., *Trichuris trichiura* and *Ascaris lumbricoides*; N3 and N4, from patients with single roundworm infections, i.e., *T. trichiura*; N5, from a patient infected with *Entamoeba histolytica*.

with increasing dilution at 1:128 dilution ratios. The 30 nm AuNPs–MαHIgG$_4$ with OD 4 showed the highest specificity when tested with various serum samples.

Acknowledgments

The authors appreciate the technical support from both the School of Materials & Mineral Resources Engineering and the Institute for Research in Molecular Medicine of USM. This research was funded by the University Research grants 1001/PSKBP/8630019 and PGRS 1001/Pbahan/8034049. The first author received a National Science Fellowship from the Ministry of Science, Technology and Innovation (MOSTI/BMI/TAJ/1-1/2 Jld. 18 (271)).

References

[1] Rasch M R, Sokolov K V and Korgel B A 2009 Limitations on the optical tunability of small diameter gold nanoshells. *Langmuir* **25** 11777–85

[2] Liu X, Dai Q, Austin L, Coutts J, Knowles G, Zou J, Chen H and Huo Q 2008 A one-step homogeneous immunoassay for cancer biomarker detection using gold nanoparticle probes coupled with dynamic light scattering *J. Am. Chem. Soc.* **130** 2780–2

[3] Kim G C, Kim G J, Park S R, Jeon S M, Seo H J, Iza F and Lee J K 2009 Air plasma coupled with antibody-conjugated nanoparticles: a new weapon against cancer. *J. Phys. D: Appl. Phys.* **42** 032005

[4] Sokolov K, Follen M, Aaron J, Pavlova I, Malpica A, Lotan R and Richards-Kortum R 2003 Real-time vital optical imaging of precancer using anti-epidermal growth factor receptor antibodies conjugated to gold nanoparticles *Cancer Res.* **63** 1999–2004

[5] Kim D, Park S, Lee J H, Jeong Y Y and Jon S 2007 Antibiofouling polymer-coated gold nanoparticles as a contrast agent for *in vivo* x-ray computed tomography imaging *J. Am. Chem. Soc.* **129** 7661–5

[6] Nguyen D T, Kim D-J and Kim K-S 2011 Controlled synthesis and biomolecular probe application of gold nanoparticles *Micron* **42** 207–27

[7] Kaur J, Singh K V, Boro R, Thampi K R, Raje M, Varshney G C and Suri C R 2007 Immunochromatographic dipstick assay format using gold nanoparticles labeled protein-hapten conjugate for the detection of atrazine *Environ. Sci. Technol.* **41** 5028–36

[8] Zhang G P, Wang X N, Yang J F, Yang Y Y, Xing G X, Li Q M, Zhao D, Chai S J and Guo J Q 2006 Development of an immunochromatographic lateral flow test strip for detection of β-adrenergic agonist Clenbuterol residues *J. Immunol. Methods* **312** 27–33

[9] Naoki N, Ryou T, Teruko Y, Tatsuro E, Kagan K, Yuzuru T and Eiichi T 2006 Gold nanoparticle-based novel enhancement method for the development of highly sensitive immunochromatographic test strips *Sci. Technol. Adv. Mater.* **7** 270–5

[10] Xiulan S, Xiaolian Z, Jian T, Zhou J and Chu F S 2005 Preparation of gold-labeled antibody probe and its use in immunochromatography assay for detection of aflatoxin B1 *Int. J. Food Microbiol.* **99** 185–94

[11] Posthuma-Trumpie G, Korf J and van Amerongen A 2009 Lateral flow (immuno)assay: its strengths, weaknesses, opportunities and threats. A literature survey *Anal. Bioanal. Chem.* **393** 569–82

[12] Tanaka R, Yuhi T, Nagatani N, Endo T, Kerman K, Takamura Y and Tamiya E 2006 A novel enhancement assay for immunochromatographic test strips using gold nanoparticles *Anal. Bioanal. Chem.* **385** 1414–20

[13] Chiao D-J, Shyu R-H, Hu C-S, Chiang H-Y and Tang S-S 2004 Colloidal gold-based immunochromatographic assay for detection of botulinum neurotoxin type B *J. Chromatogr.* B **809** 37–41

[14] Tian Z, Liu L Q, Peng C, Chen Z and Xu C 2009 A new development of measurement of 19-Nortestosterone by combining immunochromatographic strip assay and ImageJ software *Food Agricult. Immunol.* **20** 1–10

[15] Khreich P L, Boutal H, Devilliers K, Créminon C and Volland H 2008 Detection of *Staphylococcus* enterotoxin B using fluorescent immunoliposomes as label for immunochromatographic testing *Anal. Biochem.* **377** 182–8

[16] Tang X X, Liu X, Huang X, Chen Y, Wang W and Xiang J 2011 Development of a lateral flow immunoassay (LFA) strip for the rapid detection of 1-aminohydantoin in meat samples *J. Food Sci.* **76** 138–43

[17] Rodríguez-González B M, Paul L-M and Luis M 2007 An electrochemical model for gold colloid formation via citrate reduction *Z. Phys. Chem.* **221** 415–26

[18] Kumar S, Aaron J and Sokolov K 2008 Directional conjugation of antibodies to nanoparticles for synthesis of

multiplexed optical contrast agents with both delivery and targeting moieties *Nature Prot.* **3** 314–20
[19] Brown K R, Walter D G and Natan M J 2000 Seeding of colloidal Au nanoparticle solutions. 2. Improved control of particle size and shape *Chem. Mater.* **12** 306–13
[20] Brown K R and Natan M J 1998 Hydroxylamine seeding of colloidal Au nanoparticles in solution and on surfaces *Langmuir* **14** 726–8
[21] Bauer G, Hassmann J, Walter H, Haglmüller J, Mayer C and Schalkhammer T 2003 Resonant nanocluster technology—from optical coding and high quality security features to biochips *Nanotechnology* **14** 1289–311
[22] Jana N R, Gearheart L and Murphy C J 2001 Evidence for seed-mediated nucleation in the chemical reduction of gold salts to gold nanoparticles *Chem. Mater.* **13** 2313–22
[23] Maus L, Dick O, Bading H, Spatz J P and Fiammengo R 2010 Conjugation of peptides to the passivation shell of gold nanoparticles for targeting of cell-surface receptors *ACS Nano* **4** 6617–28
[24] Rahmah N *et al* 2001 Specificity and sensitivity of a rapid dipstick test (Brugia Rapid) in the detection of Brugia malayi infection *Trans. R. Soc. Trop. Med. Hyg.* **95** 601–4
[25] Jamail M, Andrew K, Junaidi D, Krishnan A K, Faizal M and Rahmah N 2005 Field validation of sensitivity and specificity of rapid test for detection of Brugia malayi infection *Trop. Med. Int. Health* **10** 99–104
[26] Grabar K C, Griffith Freeman R, Hommer M B and Natan M J 1995 Preparation and characterization of Au colloid monolayers *Anal. Chem.* **67** 735–43
[27] Siti R M, Khairunisak A R, Aziz A A and Noordin R 2012 Study on controlled size, shape and dispersity of gold nanoparticles (AuNPs) synthesized via seeded-growth technique for immunoassay labeling *Adv. Mater. Res.* **364** 504–9
[28] Link S and El-Sayed M A 1999 Size and temperature dependence of the plasmon absorption of colloidal gold nanoparticles *J. Phys. Chem.* B **103** 4212–7
[29] Horisberger M, Rosset J and Bauer H 1975 Colloidal gold granules as markers for cell surface receptors in the scanning electron microscope *Cell. Mole. Life Sci.* **31** 1147–9
[30] Chun P, Wong R and Tse H 2009 *Colloidal Gold and Other Labels for Lateral Flow Immunoassays Lateral Flow Immunoassay* (New York: Humana Press) pp 75–82
[31] O'Farrell B, Wong R and Tse H 2009 *Evolution in Lateral Flow–Based Immunoassay Systems Lateral Flow Immunoassay* (New York: Humana Press) pp 1–33
[32] Yu C Y *et al* 2011 Dry-reagent gold nanoparticle-based lateral flow biosensor for the simultaneous detection of *Vibrio cholerae* serogroups O1 and O139 *J. Microbiol. Methods* **86** 277–82
[33] Haiss W, Thanh N T K, Aveyard J and Fernig D G 2007 Determination of size and concentration of gold nanoparticles from UV–vis spectra *Anal. Chem.* **79** 4215–21
[34] Baptista P, Pereira E, Eaton P, Doria G, Miranda A, Gomes I, Quaresma P and Franco R 2008 Gold nanoparticles for the development of clinical diagnosis methods *Anal. Bioanal. Chem.* **391** 943–50
[35] Shi C, Zhao S, Zhang K, Hong G and Zhu Z 2008 Preparation of colloidal gold immunochromatography strip for detection of methamidophos residue *J. Environ. Sci.* **20** 1392–7
[36] Deng X, Gao D, Liang F, Jin D, Tian Y, Chen Y, Yu A and Zhang H 2009 Spectrophotometric determination of human immunoglobulin G based on enlargement of gold nanoparticles *Chin. J. Chem.* **27** 2363–7
[37] Yeh C-H, Hung C-Y, Chang T, Lin H-P and Lin Y-C 2009 An immunoassay using antibody-gold nanoparticle conjugate, silver enhancement and flatbed scanner *Microfluid. Nanofluid.* **6** 85–91
[38] Jiali N, Tao Z and Zhongfan L 2007 One-step seed-mediated growth of 30–150 nm quasispherical gold nanoparticles with 2-mercaptosuccinic acid as a new reducing agent *Nanotechnology* **18** 325607
[39] Pissuwan D, Cortie C H, Valenzuela S M and Cortie M B 2007 Gold nanosphere-antibody conjugates for hyperthermal therapeutic applications *Gold Bull.* **40** 121–9
[40] Huang X, El-Sayed I H, Qian W and El-Sayed M A 2006 Cancer cell imaging and photothermal therapy in the near-infrared region by using gold nanorods *J. Am. Chem. Soc.* **128** 2115–20
[41] El-Sayed I H, Huang X and El-Sayed M A 2005 Surface plasmon resonance scattering and absorption of; anti-EGFR antibody conjugated gold nanoparticles in cancer diagnostics: applications in oral cancer *Nano Lett.* **5** 829–34
[42] Link S, Mohamed M B and El-Sayed M A 1999 Simulation of the optical absorption spectra of gold nanorods as a function of their aspect ratio and the effect of the medium dielectric constant *J. Phys. Chem.* B **103** 3073–7
[43] Kelly K L, Coronado E, Zhao L L and Schatz G C 2002 The optical properties of metal nanoparticles: the influence of size, shape, and dielectric environment *J. Phys. Chem.* B **107** 668–77
[44] Norman T J, Grant C D, Magana D, Zhang J Z, Liu J, Cao D, Bridges F and Van Buuren A 2002 Near infrared optical absorption of gold nanoparticle aggregates *J. Phys. Chem.* B **106** 7005–12
[45] Ziegler C and Eychmüller A 2011 Seeded growth synthesis of uniform gold nanoparticles with diameters of 15–300 nm *J. Phys. Chem.* C **115** 4502–6
[46] Xu X-H N, Huang S, Brownlow W, Salaita K and Jeffers R B 2004 Size and temperature dependence of surface plasmon absorption of gold nanoparticles induced by tris(2,2′-bipyridine)ruthenium(II) *J. Phys. Chem.* B **108** 15543–51
[47] Bohren C F and Huffman D R 1983 *Absorption and Scattering of Light by Small Particles* (New York: Wiley)
[48] Bogatyrev V, Dykman L, Khlebtsov B and Khlebtsov N 2004 Measurement of mean size and evaluation of polydispersity of gold nanoparticles from spectra of optical absorption and scattering *Opt. Spectrosc.* **96** 128–35
[49] Choi D H, Lee S K, Oh Y K, Bae B W, Lee S D, Kim S, Shin Y-B and Kim M-G 2010 A dual gold nanoparticle conjugate-based lateral flow assay (LFA) method for the analysis of troponin I *Biosens. Bioelectron.* **25** 1999–2002
[50] Liu C, Jia Q, Yang C, Qiao R, Jing L, Wang L, Xu C and Gao M 2011 Lateral flow immunochromatographic assay for sensitive pesticide detection by using Fe_3O_4 nanoparticle aggregates as color reagents *Anal. Chem.* **83** 6778–84
[51] Tippkötter N, Stückmann H, Kroll S, Winkelmann G, Noack U, Scheper T and Ulber R 2009 A semi-quantitative dipstick assay for microcystin *Anal. Bioanal. Chem.* **394** 863–9
[52] 2006 *Rapid Lateral Flow Test Strips: Considerations for Product Development* (Bedford: Millipore Inc)
[53] Bergen en Henegouwen P M P and Leunissen J L M 1986 Controlled growth of colloidal gold particles and implications for labelling efficiency *Histochem. Cell Biol.* **85** 81–7